ARTICLE

Computational fluid dynamic analysis of bioprinted self-supporting perfused tissue models

T. J. Sego[1] | Matthew Prideaux[2,3] | Jane Sterner[4,5] | Brian Paul McCarthy[4] | Ping Li[6] | Lynda F. Bonewald[2,3,7] | Burcin Ekser[6] | Andres Tovar[8] | Lester Jeshua Smith[4,5]

[1]Department of Intelligent Systems Engineering, Indiana University, Bloomington, Indiana

[2]Indiana Center for Musculoskeletal Health, Indiana University, Indianapolis, Indiana

[3]Department of Anatomy and Cell Biology, Indiana University School of Medicine, Indianapolis, Indiana

[4]Radiology and Imaging Sciences, Indiana University School of Medicine, Indianapolis, Indiana

[5]3D Bioprinting Core, Indiana University School of Medicine, Indianapolis, Indiana

[6]Division of Transplant Surgery, Department of Surgery, Indiana University School of Medicine, Indianapolis, Indiana

[7]Department of Orthopaedic Surgery, Indiana University School of Medicine, Indianapolis, Indiana

[8]Department of Mechanical and Energy Engineering, Indiana University-Purdue University Indianapolis, Indianapolis, Indiana

Correspondence
Lester J. Smith, PhD, 950 W. Walnut Street, Room E124, Indianapolis, IN 46202.
Email: smitlej@iu.edu

Abstract

Natural tissues are incorporated with vasculature, which is further integrated with a cardiovascular system responsible for driving perfusion of nutrient-rich oxygenated blood through the vasculature to support cell metabolism within most cell-dense tissues. Since scaffold-free biofabricated tissues being developed into clinical implants, research models, and pharmaceutical testing platforms should similarly exhibit perfused tissue-like structures, we generated a generalizable biofabrication method resulting in self-supporting perfused (SSuPer) tissue constructs incorporated with perfusible microchannels and integrated with the modular FABRICA perfusion bioreactor. As proof of concept, we perfused an MLO-A5 osteoblast-based SSuPer tissue in the FABRICA. Although our resulting SSuPer tissue replicated vascularization and perfusion observed in situ, supported its own weight, and stained positively for mineral using Von Kossa staining, our in vitro results indicated that computational fluid dynamics (CFD) should be used to drive future construct design and flow application before further tissue biofabrication and perfusion. We built a CFD model of the SSuPer tissue integrated in the FABRICA and analyzed flow characteristics (net force, pressure distribution, shear stress, and oxygen distribution) through five SSuPer tissue microchannel patterns in two flow directions and at increasing flow rates. Important flow parameters include flow direction, fully developed flow, and tissue microchannel diameters matched and aligned with bioreactor flow channels. We observed that the SSuPer tissue platform is capable of providing direct perfusion to tissue constructs and proper culture conditions (oxygenation, with controllable shear and flow rates), indicating that our approach can be used to biofabricate tissue representing primary tissues and that we can model the system in silico.

- -

1 | INTRODUCTION

The ability to use biofabrication to accurately recreate natural tissues and replicate their in situ environment in vitro with bioreactors will lead to tissues which can (a) serve as accurate research models of tissue activity, (b) act as early stage human tissue testing platforms for pharmaceuticals in development without the need for confounding animal models, (c) potentially produce implantable tissues for clinical use, and (d) possibly serve as testing platforms for animal humanization used to develop xenotransplants.

Like cells in natural tissues in situ, cells in biofabricated tissues require consistent and adequate perfusion for nutrient-dependent cell metabolism, differential signaling, extracellular matrix (ECM) deposition, and removal of metabolite wastes (Bonfiglio, Leungcha-vaphongse, Repetto, & Siggers, 2010; Dimmeler, Haendeler, Ripp-mann, Nehls, & Zeiher, 1996; Gan, Miocic, Doroudi, Selin-Sjöögren, & Jern, 2000; Kang & Chang, 2018). Natural tissues are comprised of integrated vasculature by which cells in the tissue are perfused with nutrient-rich blood. Tissue vasculature is further integrated with the cardiovascular system, which drives nutrient perfusion. Generating biofabricated tissues exhibiting similar distributed vasculature-like structures integrated with a system capable of driving perfusion, however, has proved to be an engineering, biological, and practical challenge (Ball, Nguyen, Placone, & Fisher, 2016; Egger et al., 2017; Goldstein, Juarez, Helmke, Gustin, & Mikos, 2001; Stiehler et al., 2009; Wang, Wu, Wang, Lin, & Sun, 2009; Warren et al., 2009; Wu & Ringeisen, 2010), which must be overcome to generate in vivo-like tissue structures (Carrier et al., 2002; Dennis, Smith, Philp, Donnelly, & Baar, 2009; Guller, Grebenyuk, Shekhter, Zvyagin, & Deyev, 2016; Maidhof et al., 2012).

Impeller-driven spinner flask bioreactors provide perfusion by flowing media over the tissue construct, which results in poorly controlled and poorly defined perfusion to tissues within the bulk of tissues or result in no perfusion within the bulk of solid tissues (Radisic et al., 2004; Sikavitsas, Bancroft, & Mikos, 2002). In addition, vortex breakdown may result in uneven mixing, resulting in uneven nutrient distribution (Dusting, Sheridan, & Hourigan, 2006). Hollow fiber bioreactors are comprised of perfusible, semipermeable hollow fibers enveloped within a cartridge filled with cells and media. As media flows through the fibers, there is a nutrient exchange between the fibers and the cartridge space such that fresh nutrients transferring into the cartridge are available to the cells and waste from the cells are transferred out of the cartridge, and carried away from the culture environment (Ye, Xia, Ferguson, Triffitt, & Cui, 2007; Zhou, Shen, & Lauschke, 2019). While this approach does provide controlled cellular perfusion, it is not suitable for solid tissues with 3D structures, which then need to be removed from the bioreactor. Direct perfusion into porous tissues applies perfusive flow directly to the open pores on the surface and through the bulk of a 3D tissue construct (Egger et al., 2017; Gelinsky, Bernhardt, & Milan, 2015). For constructs with nonuniform pore sizes and randomly oriented pores, there are unknown flow paths, unknown conduit dimensions, and unknown or poorly defined conduit shapes, thus increasing the likelihood of producing unwanted turbulent flow, subnutritious flow fields, and uneven nutrient distribution. For direct perfusion to constructs with uniform pore sizes, the fact that the constructs are scaffold-dependent means that flow may be satisfactory but the cell concentration is lower than what is observed in natural tissue, thus limiting the construct's suitability as a tissue (Moldovan, 2018). Rotating vessel bioreactors keeps tissue constructs in the medium filled vessel in a constant state of freefall by keeping the drag, centrifugal, and gravitational forces in equilibrium, thereby providing low shear stresses and high mass transfer rates (Porter, Lin, Peister, Hutmacher, & Guldberg, 2007). The drawback to using them with porous materials is the same as those presented by spinner flasks. Compression bioreactors are also capable of promoting flow in tissue constructs (Gelinsky et al., 2015; Kim, Sah, Grodzinsky, Plaas, & Sandy, 1994). However, this method is most suitable to tissues normally subjected to compression (musculoskeletal tissues) and the force/strain (as much as 10%; Kim et al., 1994) of compression may also result in damage or disintegration of initially delicate scaffold-free tissues.

We have developed the scaffold-free self-supporting and per-fused (SSuPer) tissue method, whereby a perfusion module guides nutrient flow directly into an array of microchannels built into the tissue construct. Since the microchannels exhibit diameters and flow paths prescribed by the tissue designer, our approach provides direct and distributed nutrient perfusion to tissues within the tissue bulk. The controlled diameter and flow path of the tissue microchannels allow for accurate modeling of perfusion within the tissue construct at different flow rates, with different flow media (i.e., blood, cell culture media, etc., also described as "media of interest") and for different culture conditions (oxygen concentration, temperature, flow rate, etc.). Furthermore, the SSuPer tissue design produces scaffold-free tissues comprised only of cells embedded within their own cell-secreted ECM, reproducing the composition and structure of natural tissues, whereas other 3D biofabrication approaches are normally comprised of reconstituted or synthetically derived matrices, which limits their ability to integrate with the host tissue.

In this proof of concept, we describe how we used the SSuPer tissue method to fabricate a SSuPer bone-like tissue. Challenges with our first trial indicated that computation-based analysis could help guide our tissue design (channel diameter and pattern) and bioreactor implementation (flow rate, flow direction, and SSuPer tissue integration with the bioreactor). Our goals are to (a) introduce SSuPer tissues as a new method for generating generalizable, fully

perfusible scaffold-free tissue constructs, (b) demonstrate that we can generate, perfuse, and culture, SSuPer tissues exhibiting perfusible microchannels exhibiting a range of patterns and diameters and, (c) with a computational model, demonstrate that we can computationally model oxygen diffusion through SSuPer tissue as a function of medium perfusion.

2 | METHODS

2.1 | Biofabrication (bioprinting, construction, and culture) and analysis of a 3D-bioprinted SSuPer tissue

As a proof of concept, a SSuPer bone tissue construct with various channel diameters (Figure 1) was bioprinted and continuously perfused for 2 weeks. Briefly, a Kenzan platen with perforations in a 9 × 9 pattern was modified to serve as a base for the tissue constructs (Figure 2a,b). The platen was aseptically coated with 0.15 mg/ml collagen (Rat Tail Collagen Type 1; Becton Dickenson Laboratories, Bedford, MA) for 1 hr, aspirating unbound collagen, and allowing the platen to air dry for at least 1 hr before use. This platen was then slotted onto a Kenzan needle array through its micro-channels (Figure 2c,d) and then used for bioprinting tissue constructs from cellular spheroids into tissue constructs (Figures 3 and 4; Aguilar, Smith et al., 2019; Moldovan, Hibino, & Nakayama, 2017; Smith, Li, Holland, & Ekser, 2018).

Tissue constructs were made using cell aggregates (spheroids) made from murine MLO-A5 cells. MLO-A5 cells are late osteoblasts, which produce large amounts of collagen that mineralizes into a bone-like structure in culture (Kato et al., 2001). Briefly, 12,000 to 13,000 cells/well were seeded into 96-well plates with α-modified Eagle's medium (α-MEM) plus 10% fetal bovine serum (FBS) and 1%

penicillin/streptomycin (control medium). The cells were then allowed to coalesce for 48–72 hr into 500-μm diameter spheroids (Moldovan et al., 2017). Construct design was achieved using the Regenova (Cyfuse K.K., Japan) Bio 3D Printer's construct design feature. Following spheroid formation and construct design, the Regenova bioprinter was used to bioprint/biofabricate a scaffold-free 3D tissue construct as described by Aguilar, Smith, et al. (2019) and Smith et al. (2018). Briefly, Regenova's computer vision system selects a suitable spheroid and the bioprinter's mobile nozzle is then moved close to the spheroid and negative pneumatic back pressure is used to secure the spheroid to the nozzle tip and pick the selected spheroid from the 96-well plate. The nozzle is then moved over the Kenzan (a microneedle array being used as a temporary support) and then lowered to a predetermined height on a predetermined needle positioned on the 9 × 9 Kenzan needle array according to the predetermined construct design. Pneumatic back pressure is then released from the nozzle, releasing the spheroid, which stays in position on the Kenzan needle array at the designated height. Spheroids were thus bioprinted onto the Kenzan to form three to four spheroid high constructs with cross-sectional pattern, as shown in Figure 1. It should be noted that the terms "scaffold" or "scaffold-dependent" in bioprinting and biofabrication contexts are normally used to describe cells embedded within ECM surrogate scaffolds such as polymers or reconstituted proteins (i.e., collagen) or any non-cell material within the tissue that is not secreted from the cells (Moldovan, 2018; Moldovan et al., 2017; Ozbolat, 2015). The scaffold-dependent tissue is therefore dependent on these scaffolds to hold the tissue together over the long-term. On the other hand, scaffold-free is normally used to describe tissues that are comprised of cells embedded within their own cell-secreted matrix (not contrived or reconstituted ECM scaffolds) and are therefore "scaffold-free" (Aguilar, Olivos et al., 2019; Aguilar, Smith et al.,
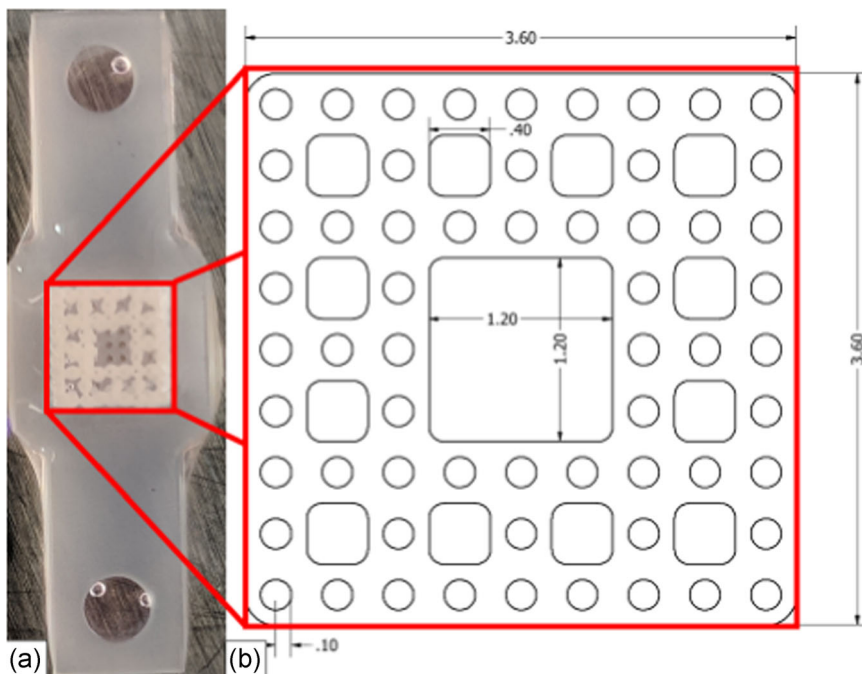

FIGURE 1 Self-supporting perfused (SSuPer) tissue with various microchannel sizes adhered to top platen. (a) The SSuPer tissue (white) on the top platen (gray) has 200-, 400-, and 1,200-μm wide channels. (b) A larger diagram of the tissue construct showing channel sizes and patterns [Color figure can be viewed at wileyonlinelibrary.com]
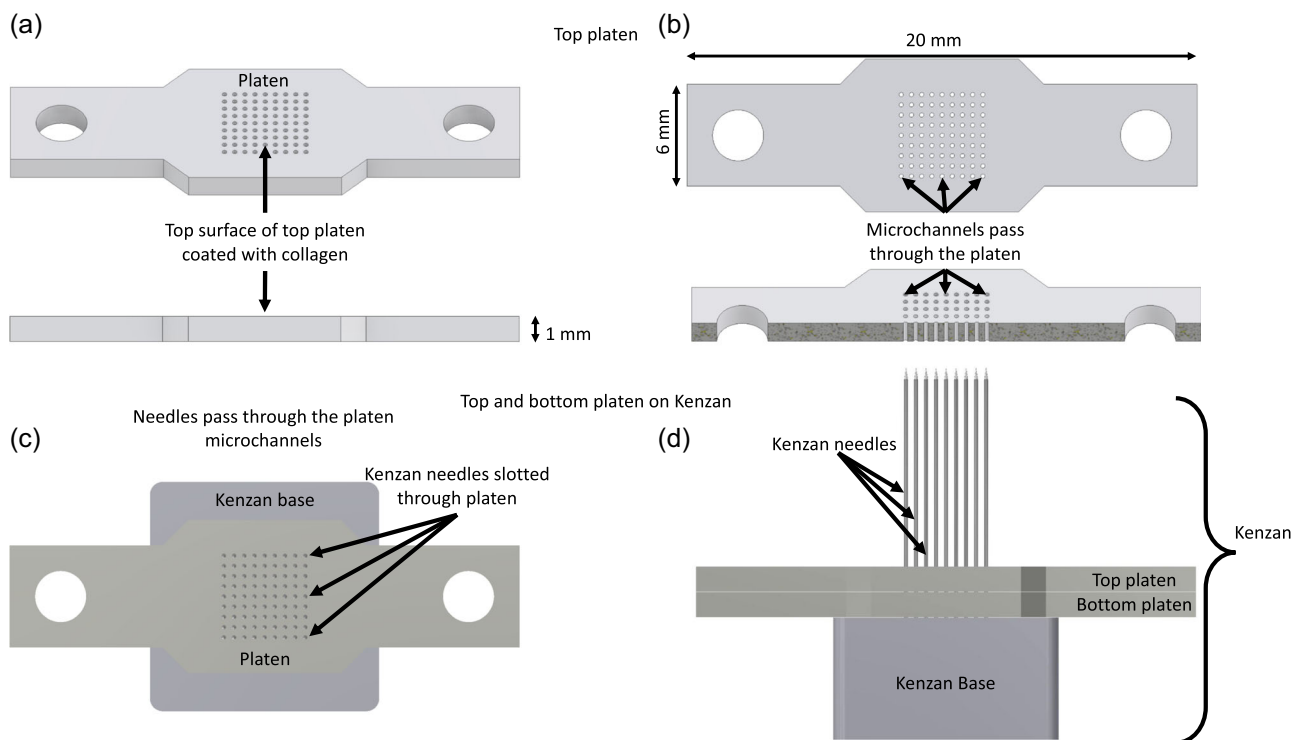
FIGURE 2 The top platen is used to align microchannels in bioprinted tissues and guide flow into microchannels during perfusion. (a) The top of the top platen is coated with collagen to facilitate cellular spheroid adhesion. (b) Microchannels pass through the platen and can facilitate needles or flow. (c,d) For bioprinting the SSuPer tissues, the platens can easily be slotted over the needles of the Kenzan base. SSuPer, self-supporting perfused [Color figure can be viewed at wileyonlinelibrary.com]

2019; Blakely, Manning, Tripathi, & Morgan, 2015; Itoh et al., 2015; Moldovan, 2018; Moldovan et al., 2017; Murata et al., 2015; Ozbolat, 2015; Toratani et al., 2017). The distinction between scaffold-dependent and scaffold-free can similarly be defined by the tissue's final composition after maturation. Since the tissues are removed from the needles in the Kenzan method after maturation and the needles are not serving as ECM surrogates, the Kenzan method is, by definition, a scaffold-free method. The distinction is important since the scaffold-free Kenzan method results in self-generated tissue structures in a manner similar to natural tissue, unlike the scaffold-dependent method.

After incubating for 2 days, the collagen-coated top-platen was slid into contact with the construct (Figure 3d–f), facilitating adhesion of cells in the bottom layer of spheroids to ensure adherence of the construct to the collagen-coated platen. The constructs are then allowed to adhere to the collagen-coated platen for 3 days of culture as the spheroids fused (Figure 3g–i). With the construct still adhered in place, the platen was removed from the Kenzan, leaving a SSuPer tissue construct with perfusible microchannels (Figure 3j,k; construct feature dimensions are provided in Supporting Information Material). While the larger diameter microchannels (400 and 1,200 μm) are achieved by the specific spheroid placement, the 200-μm diameter microchannels are a result of the spaces left by the Kenzan needles after Kenzan removal, which approximate the diameter of Haversian Canals (Cvetkovic et al., 2013). It should be noted, however, that the

SSuPer tissue method is intended to be generalizable to several tissue types, not just bone. The 200-μm microchannels are also aligned with, and contiguous with, the channels in the supporting platen, therefore serving as conduits for medium transport. During the initial 5 days after bioprint, the spheroids also fused with one another, forming an intact single tissue construct. Upon removal from the Kenzan, the platen with the attached construct was removed from the needles and secured, construct-side-up, to a custom perfusion module and placed in a FABRICA Bioreactor Platform (Smith et al., 2018) so that medium can flow through the FABRICA's integrated perfusion channels (Smith et al., 2018) and perfuse the construct (Figure 4a–d). For 2 weeks, a peristaltic pump connected to the FABRICA was used to perfuse osteogenic cell culture media composed of α-minimum essential medium (α-MEM) supplemented with 10% serum, 4–5 mM β-glycerophosphate, and 100 ug/ml ascorbate at 0.5 ml/min. Culture medium was exchanged twice a week during perfusion. After perfusion, the SSuPer tissue was fixed with 4% formalin, removed from the platen, embedded in optimal cutting tempera-ture (OTC) medium, and frozen. The frozen samples were cut 5–10 μm thick, and stained with hematoxylin and eosin and Von Kossa. Briefly, Von Kossa staining for phosphate deposits was achieved by rinsing the sections with water, incubating the sections with 1% silver nitrate under ultraviolet light, followed by rinses with water and sodium thiolsulfate. Phosphate deposits show up at black stains (Kato et al., 2001).
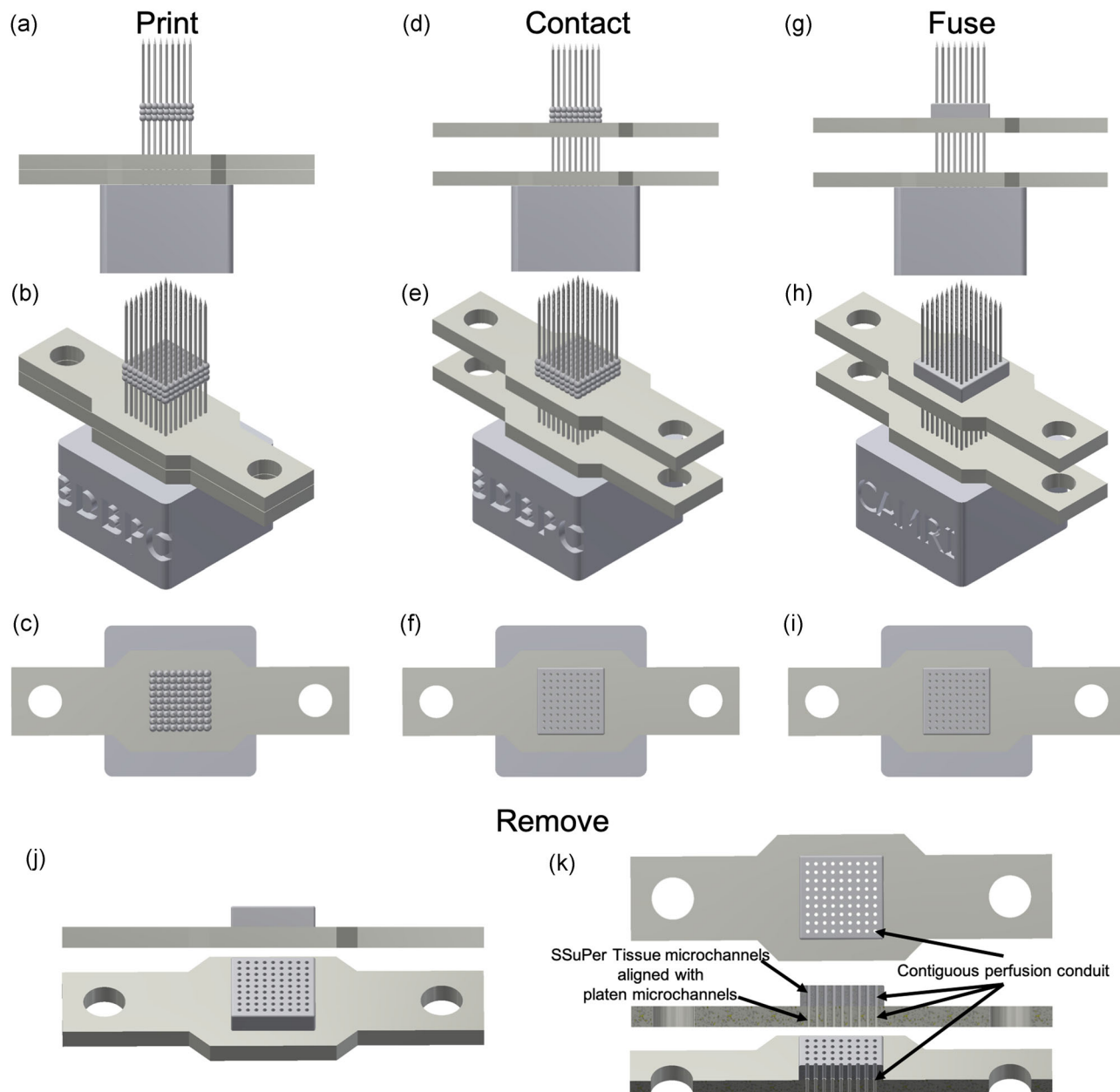
FIGURE 3 SSuPer tissue biofabrication onto the Kenzan with the Regenova Bio 3D printer. (a–c) In the print step, the Regenova places spheroids onto the Kenzan needles in a preselected pattern and are held in place by friction. (d–f) After 2 days, as the spheroids fuse, the platen is slotted into contact with the forming tissue construct such that cells in the construct adhere to the collagen coating on the platen. (g–i) The spheroids fully fuse, forming a tissue construct on the platen. (j, k) With the spheroids fully fused into a tissue construct and adhered to the top platen, the tissue-platen complex is removed from the Kenzan base with the holes left in the construct from the Kenzan needles forming perfusible microchannels aligned and contiguous with the microchannels in the platen. The resulting construct is a SSuPer tissue. SSuPer, self-supporting perfused [Color figure can be viewed at wileyonlinelibrary.com]

2.2 | Tissue model design for computational fluid dynamics analysis

SSuPer tissue models with representative microchannel patterns shown in Figure 5a–e were generated using Autodesk Inventor (Autodesk, Inc., CA) in silico as .ipt files and converted to .stl files. The channel patterns included a design with 81 channels, each 200 μm in diameter, square-packed in a 9 × 9 arrangement and spaced 400 μm apart, to a design with 1 channel 2.0 mm in diameter. Specific pattern dimensions are provided in the Supporting Information Material. Each SSuPer tissue design had the same overall dimensions of 1 mm × 3.6 mm × 3.6 mm (Figure 5f). The pattern designs represent axis-symmetric tissue design cross-sections currently possible with the Regenova Bio 3D printer (Cyfuse, Japan). Although the tissue construct patterns were changed, the pattern of the Kenzan platen's underlying perfusion microchannels was kept to the same 9 × 9 pattern.

(a)

(b)

(c)

(d)
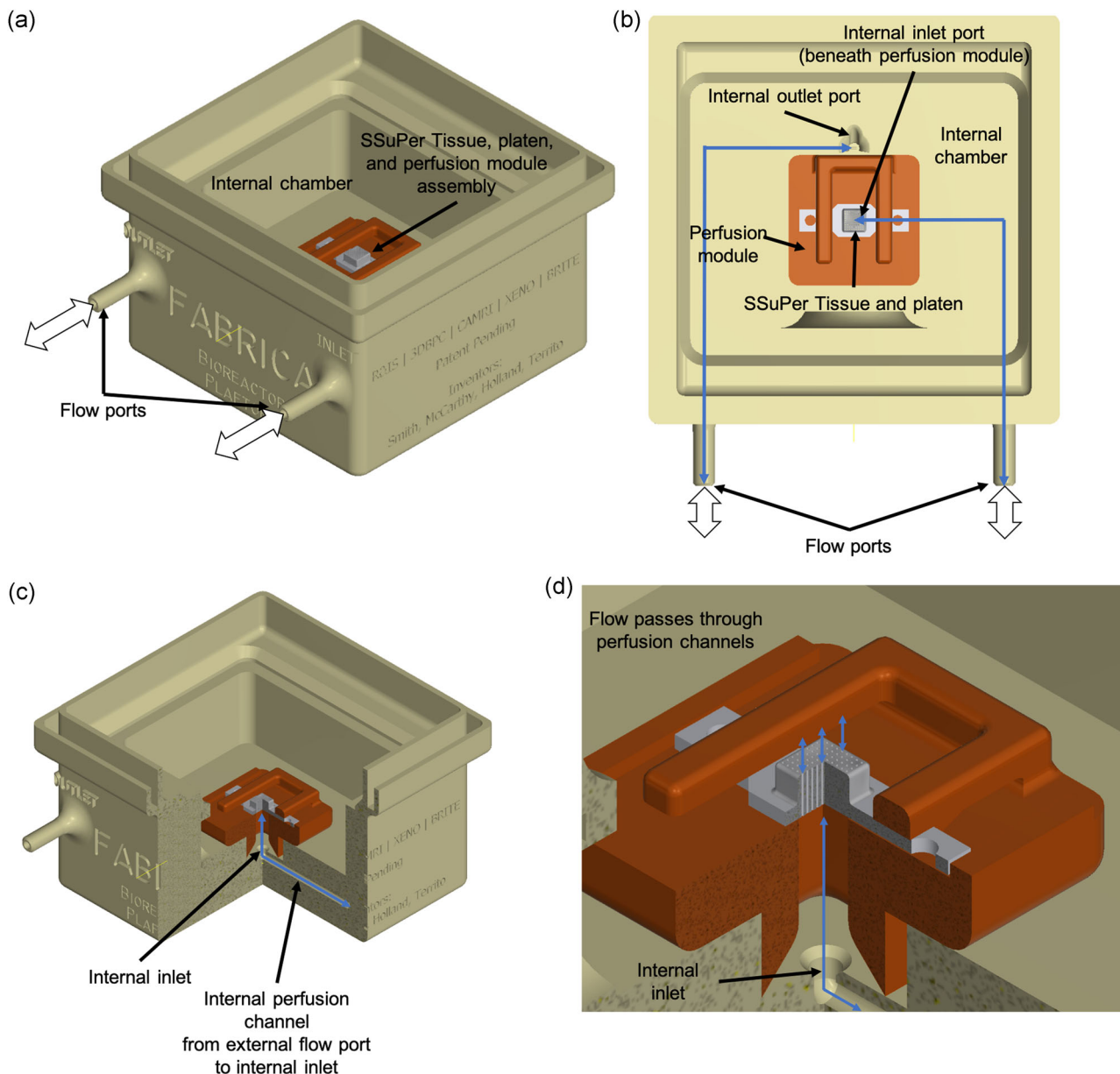
FIGURE 4 The SSuPer tissue and its integrated perfusion microchannels are perfused in the FABRICA Bioreactor platform for weeks at a time. (a) A perfusion module is secured in the flow path within the FABRICA internal chamber and the platen containing the SSuPer tissue is secured to the perfusion module. Flow ports lead to and from the peristaltic pump. (b) Flow passes into and out of the internal chamber through internal channels (blue arrows). (c) and (d) are cutaways and close-ups showing the path media flows to perfuse through the SSuPer tissue. Flow can travel into our out of the internal inlet, depending on desired flow direction. SSuPer, self-supporting perfused [Color figure can be viewed at wileyonlinelibrary.com]
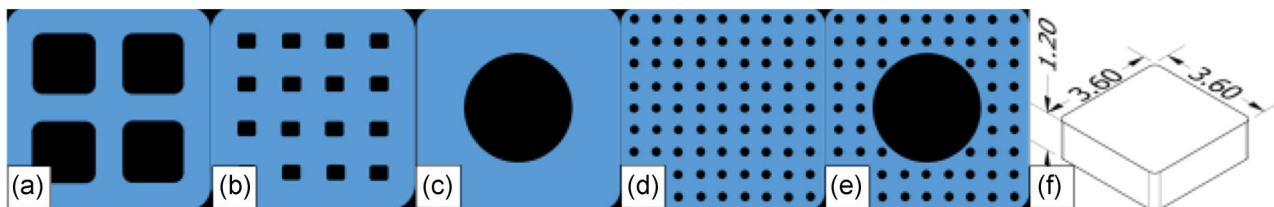
FIGURE 5 Proof-of-concept SSuPer tissue. (a) Bioprinted proof-of-concept SSuPer bone tissue after removal from Kenzan needle array. (b) Bioprinted tissue design and dimensions. SSuPer tissue microchannel patterns. (a) 4-channel pattern. (b) 16-channel pattern. (c) 1-channel pattern. (d) 81-channel pattern. (e) Hybrid pattern. (f) Orthogonal view with overall tissue dimensions. All units are in mm. SSuPer, self-supporting perfused [Color figure can be viewed at wileyonlinelibrary.com]
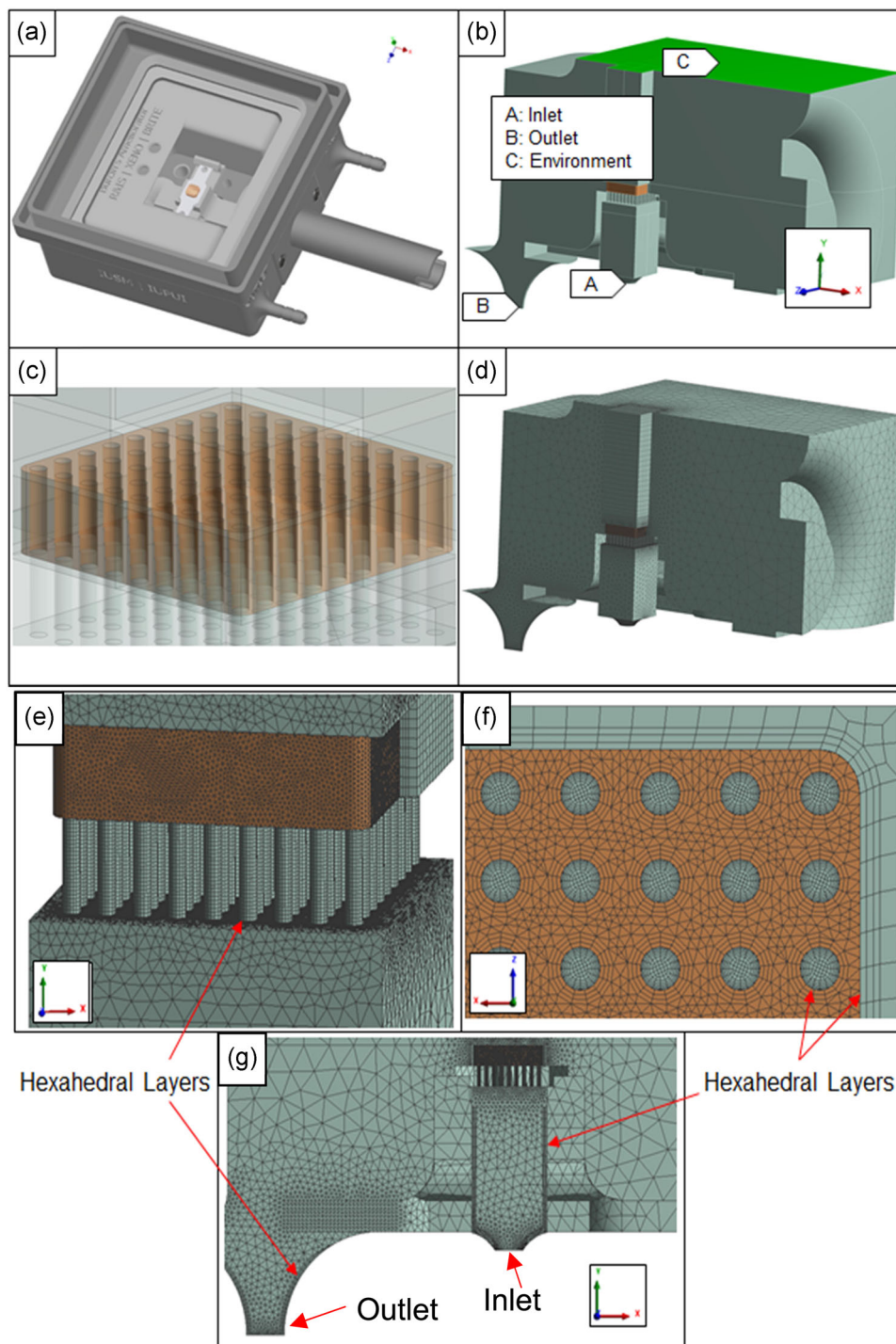
FIGURE 6 Model setup. (a) Original FABRICA CAD design with a bioprinted SSUPer tissue construct mounted within. (b) Cutaway view of computational domain derived from original CAD design, with labeled boundary surfaces (inlet, outlet and environment). (c) Detailed view of subdomain for the construct, for the case of 81 flow channels. (d) Cutaway view of computational domain mesh for representation of fluid flows. (e) Select views of model mesh. The flow domain is shown in yellow, and the construct domain is shown in green. (f) Detailed view of flow channels through the platen. (b) Detailed view of channels through the construct, for the case of 81 flow channels. (g) Detailed view of inlet and outlet regions of the flow domain. SSuPer, self-supporting perfused [Color figure can be viewed at wileyonlinelibrary.com]

2.3 | CFD analysis

2.3.1 | Model and mesh

The three-dimensional model, including the FABRICA bioreactor (Smith et al., 2018) and the SSuPer tissue perfusion model, was imported into Ansys v.16 (ANSYS, Inc., PA; Figure 6a–g), for analysis using CFX simulation suite. Separate model geometries were generated for the tissue construct/bioreactor and flow domain. Fluid–solid interactions were not included in this model and the construct was modeled as a rigid solid without surface defects and perfectly bonded to the platen. To simulate cellular respiration, a uniform oxygen source rate was applied to the construct domain. Advection in the flow domain was modeled assuming laminar flow and the system was numerically solved for steady-state conditions. Five boundaries for the flow domain were identified, each with separate boundary conditions:

1. The interface with the construct, where the condition of no fluid flow was applied.
2. An arbitrarily selected cross-section of the bioreactor-SSuPer tissue inlet flow path, where normal flow rate and oxygen concentration were specified as design parameters.
3. An arbitrarily selected cross-section of the bioreactor-SSuPer tissue outlet flow path, where normal flow rate and oxygen concentration were calculated.
4. The interface with the environment of the bioreactor-SSuPer tissue, where the condition of no normal flow was applied and oxygen concentration was specified as a design parameter.
5. The interface with all parts of the bioreactor-SSuPer tissue, where the conditions of no fluid flow or normal oxygen transport were applied.

To characterize flow behavior in the FABRICA bioreactor and within the 3D-bioprinted tissues, (a) inlet flow rates were simulated at logarithmic intervals of 0.1, 0.5, 1.0, 5.0, and 10 ml/min, representing a broad range of flow rates possible in the FABRICA system for all media of interest (Table 1) and atmospheric oxygen inputs of 9.4 mol/m^3 (21% oxygen at standard temperature and pressure), (b) shear stress at the construct interface was measured in all flow channels along the direction of flow in the normal plane halfway through the construct, the mean and standard deviation of which were recorded, (c) differential pressure across the entire SSuPer tissue was calculated by measuring the relative pressure at the FABRICA inlet and outlet and oxygenation of the construct was determined by recording the mean and standard deviation of oxygen concentration throughout the construct domain. To quantify construct stability, the net force exhibited by fluid flow on the construct was calculated and recorded. Two flow direction scenarios were analyzed. The forward (first) flow direction involved the flow medium traveling through the platen and into the construct (from inlet to outlet). Backwards (second) flow involved the flow medium traveling initially through the construct and then through the platen (from outlet to inlet).

Mapped meshing and mesh refinement were performed throughout the model using tetrahedral and hexahedral elements (Figure 6d–g). To capture the diffusive flux of oxygen into the construct, as many as three columnar layers of thin hexahedral elements were extruded into the construct from the interface with the flow channels. Thin, hexahedral elements were also extruded into the flow channels to capture the development of boundary layers according to typical laminar flow in pipes. Layers of hexahedral elements were also mapped to, and extruded from, the interface of the construct not in contact with the flow channels, to capture oxygen transport between the construct and chamber of the FABRICA. Thin elements were extruded into the flow domain from boundaries near the inlet and outlet of the FABRICA, to capture highly directional flow in these regions. The mesh consisted of a total of between 800,000 (one channel) and 1,050,000 nodes (81 channels).

2.3.2 | Material properties

Diffusivity of oxygen in the construct and all fluids of interest (media) were taken from the literature (Table 1), and construct metabolic activity was calculated using data reported in the literature for average oxygen consumption rates of human cells ([25 attomol O_2/cell/s]; McMurtrey, 2016) and a cellular density of 12k cells per spheroid of 500 µm diameter. Properties, including density, dynamic viscosity, and oxygen diffusivity for all three media fluids were

TABLE 1 Material properties

Working fluid	Density (kg/m^3)	Dynamic viscosity (mg·m^{-1}·s^{-1})	O_2 diffusivity (µm²/s)
Water	993.3 ("Viscosity of Water," 2018)	691.2 ("Viscosity of Water," 2018)	~3,300 (Ferrell & Himmelblau, 1967)
Cell culture medium + 10% FBS	1,000	940.0 (Fröhlich et al., 2013)	2,690 (Zhang et al., 2014)
Blood	~1,060 (Sniegoski & Moody, 1979)	2,798 (Anton Paar, n.d.)	1,620 (Goldstick, Ciuryla, & Zuckerman, 1976)
	Density (kg/m^3)	O_2 consumption rate (µmol·m^{-3}·s^{-1})	O_2 diffusivity (µm²/s)
Construct	1,000	458.4 (McMurtrey, 2016)	2,500 (McMurtrey, 2016; Zahm et al., 2010)

Abbreviation: FBS, fetal bovine serum

retrieved from the literature as previously reported (Fröhlich et al., 2013). For values cited in the literature reporting kinematic viscosity, the dynamic viscosity was calculated as the kinematic viscosity multiplied by the fluid density. The construct was assumed to have a density slightly greater than water (Table 1).

3 | RESULTS

3.1 | Bioprinted SSuPer tissue

The SSuPer construct remained on the platen after Kenzan removal (Figure 7a), during placement onto the perfusion module within the FABRICA. The SSuper tissue was supporting its own weight throughout Kenzan removal, transfer, placement, and perfusion (Figure 7a,b). After 2 weeks of perfusion, the SSuPer tissue continued to remain intact and support its own weight but was partially separated from the platen (Figure 7c). The lifted portion was also supporting its own weight even after removal from the culture medium (Figure 7d). Histological sections exhibited Von Kossa staining indicative of phosphate deposition in regions associated with the 200-μm microchannels left by the needles (Figure 7e). Preliminary studies, not shown, indicate that the channels remain patent throughout the incubation period. Thus, it is likely the

microchannels collapsed during histological preparation. The center of some of these Von Kossa stained features were spaced approximately 400 μm from one another, commensurate with the spacing of the 200 μm microchannel spacing of the platen and tissue patterns. The larger 400-μm and 1,200-μm diameter perfusion channels in the SSuPer tissue did not exhibit Von Kossa staining.

3.2 | Shear stress

Shear stresses generated in the CFD model of the 3D tissue microchannels were dependent on construct design, channel diameter, and flow velocity. The two lowest maximum magnitudes of shear stress in the mid-plane among all trials were measured in the four-channel construct at 0.1 ml/min in the forward (flow from internal inlet to internal outlet or flow in the +y direction; 2.270 mPa) and reverse (flow from internal outlet to internal inlet or flow in the −y direction; 2.243 mPa) directions, while the greatest two were achieved in the 81 channel constructs at 10 ml/min in the forward (2.610 Pa) and reverse (2.583 Pa) directions. Shear stresses were observed to be uniform throughout the channels of the 81-channel design, except at the upper-most surface of the construct. Significant gradients were observed near the platen channels for all other designs and both flow directions (Figure 8a,b) due to the sudden
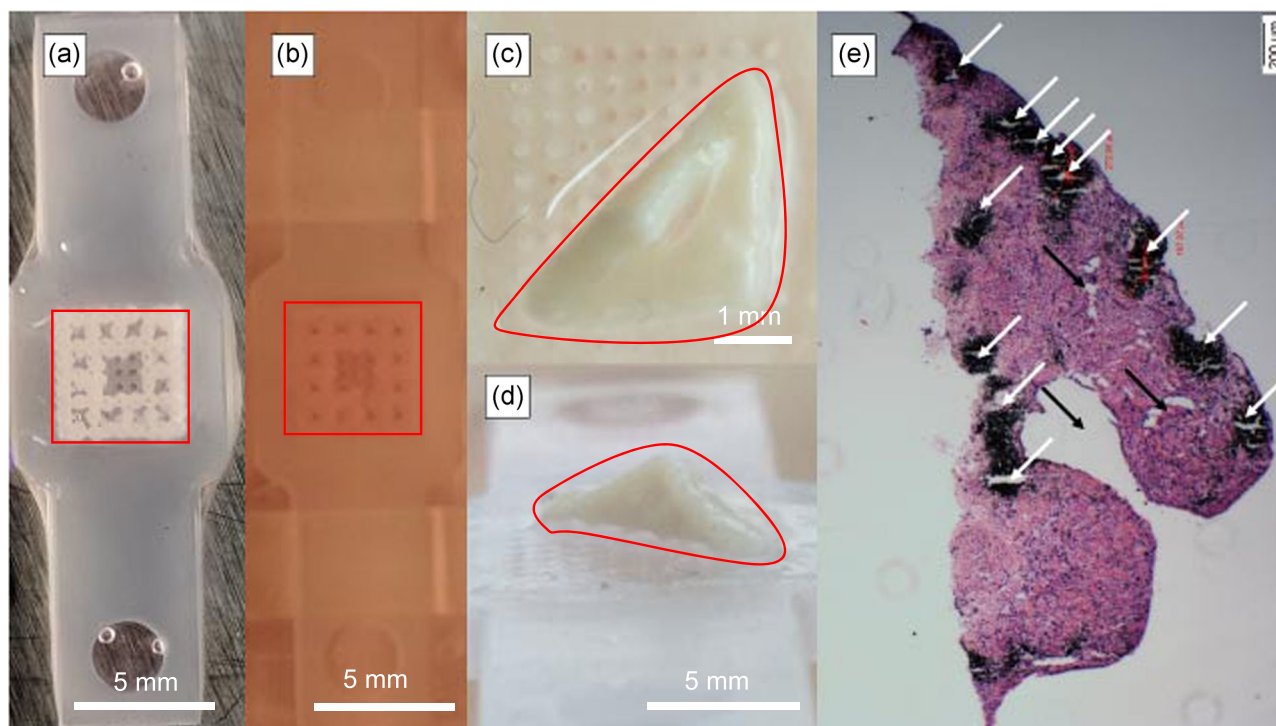

FIGURE 7 3D-Bioprinted SSuPer tissue. The tissue is outlined in red in Figure 4a–d. (a) SSuPer tissue on the platen following removal from the Kenzan but before perfusive culture. (b) SSuPer tissue installed in perfusion module within FABRICA bioreactor just before perfusive culture. (c) The SSuPer tissue partially lifted from platen as shown from the top down view after 2 weeks of perfused culture. (d) The SSuPer tissue after 2 weeks of perfused culture in the FABRICA shown from the top view is capable of supporting its own weight after removal from the bioreactor. The left corner is being supported by the tissue's mechanical integrity. (e) Histological section of SSuPer tissue. Black regions marked with white arrows are Von Kossa stained for phosphate and represent the 200-μm microchannels. Regions marked by black arrows are presumed to be microchannels without mineralization. SSuPer, self-supporting perfused [Color figure can be viewed at wileyonlinelibrary.com]

change in flow path to/from the platen. As such, gradients were more widespread on construct surfaces with increasing flow rate for all designs except the 81-channel. This was particularly true in the forward direction, where Eddy currents were observed in the construct channels. In the most extreme case, Eddy currents (turbulent flow) occupied approximately half the length of the construct channels for the 16-channel design at 10 ml/min (Figure 8c), while turbulence only occurred at the upper-most surface of the construct for the same flow rate and reverse direction (Figure 8d).
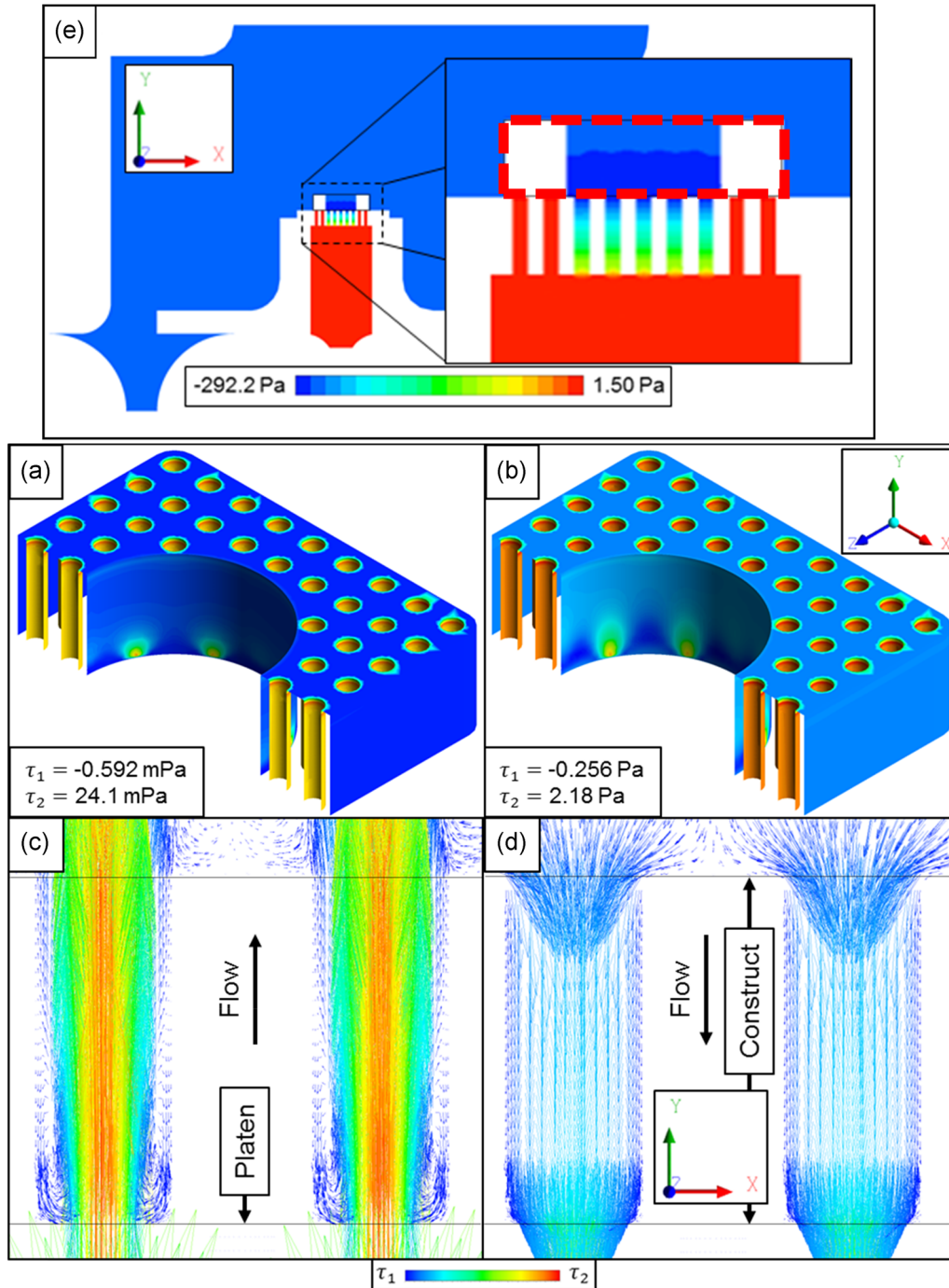
FIGURE 8 Shear stress on surfaces of the construct along the **y**− direction, for hybrid microchannel design perfused with α-modified Eagle's medium (α-MEM) and forward inlet flow rates of 0.1 ml/min (a) and 10 ml/min (b). Detailed view of velocity vectors for flow through two channels for 16-channels, α-MEM and 10 ml/min. Inlet flow in the forward (c) and reverse (d) directions. Eddy currents formed across approximately half the length of the channels in the forward direction. (e) Gauge pressure distribution in the **xy**− plane for one flow channel construct, α-MEM and 10 ml/min forward inlet flow. The construct in the inset is outlined by the dotted red line [Color figure can be viewed at wileyonlinelibrary.com]

3.3 | Pressure

Gauge pressure was calculated and recorded for all construct designs, fluids of interest, flow rates, and directions. Results showed an expected pressure drop across the flow channels in the platen and construct. For construct designs with sudden changes in flow path, no significant pressure gradients were observed for all fluids and flow rates and directions. However, for construct designs that blocked some flow paths of the platen, blocked platen channels induced additional upward forces on the construct for flow in the forward direction, contributing to compromising construct stability (Figure 8e).

3.4 | Oxygen

Oxygen distribution through the construct and medium volume (Figure 9a–d) was saturated for all designs and flow rates. The mean and standard deviation of specific oxygen throughout the construct were calculated and recorded. The mean oxygen minus three standard deviations was compared to the inlet specific oxygen, the ratio of which was used as an oxygenation metric. Varying microchannel pattern, flow rate, and direction, the least efficient configuration was the single channel for 0.1 ml/min in the forward direction (oxygenation metric of 0.9929), while the most efficient was
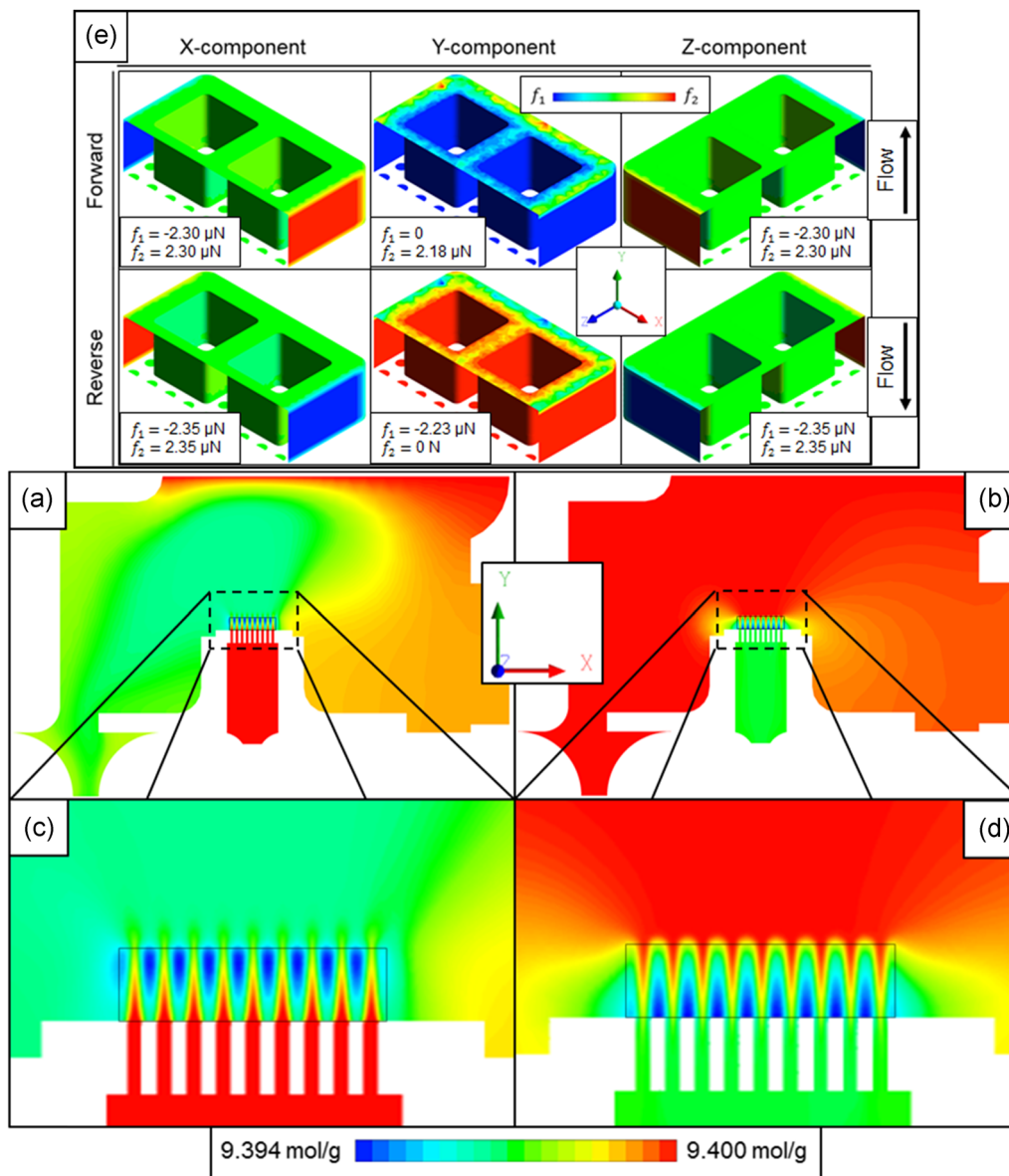
FIGURE 9 Relative oxygen distribution in the $xy-$ plane for an 81-channel construct perfused with α-MEM at an inlet flow rate of 0.1 ml/min in the forward (a) and reverse (b) directions. Note the gradual decrease in oxygen concentration along the length of the construct microchannels as well as difference in minimum and maximum oxygen levels throughout the distribution, which varies by less than 1%. (c) and (d) are magnifications of (a) and (b), respectively. (e) Forces on a construct with a four-channel design, α-MEM, and 10 ml/min flow along the $x-$ (left), $y-$ (middle), and $z-$ (right) directions, for forward (top) and reverse (bottom) flow. Images of other patterns are available in the Supporting Information Material. α-MEM, α-modified Eagle's medium [Color figure can be viewed at wileyonlinelibrary.com]

the hybrid design for 10 ml/min in the forward direction (oxygenation metric of 0.9996). Varying fluid, flow rate, and direction for the 81-channel design, the least efficient configuration was blood for 0.1 ml/min in the reverse direction (oxygenation metric of 0.9990), and the most efficient was water for 10 ml/min in the forward direction (oxygenation metric of 0.9996).

3.5 | Force distribution

Force distributions on all construct surfaces were calculated and evaluated to determine factors affecting construct stability (Figure 9e). Variations were observed in the distribution of vertical $(y-)$ forces on the top (xz-planar) surface of construct for both flow directions, while the primary forces lateral to channel flow were uniformly distributed over the external, vertical (xy− and yz-planar) surfaces of the construct. Comparing vertical force distributions for the same flow rate and opposite directions, distributions were

comparable but of opposite sign, implying that construct stability may be primarily due to construct design and resulting flow, as well as flow direction.

Select scalar measurements of simulation configurations provided quantitative insights into the effects of channel design and flow rate and direction on construct stability and viability (Figure 10). Anticipated changes in direction, shear stress, and net force along the vertical axis were observed. For the 16-channel design, the effects of Eddy currents were clearly observed for forward flow at 10 ml/min, where turbulent flow occupied over half the length of the channels and caused negative shear forces at the mid-height of the construct (Figure 10a,d). Otherwise, measured shear stress in the channels behaved predictably, with increases proportionate to channel flow speed. Measured pressure drop across the SSuPer tissue exhibited a slightly nonlinear response but was below 0.5 kPa for all simulated configurations (Figure 10b). The nonlinear behavior of the pressure drop likely occurred due to the combination of turbulence within the construct channels, as well as changes in flow throughout the bioreactor-SSuPer tissue complex.

FIGURE 10 Scalar metrics of interest for α-MEM in the forward (solid, circles) and reverse (dashed, squares) directions and all construct designs (light blue: 81 channels, orange: 16 channels; gray: four channels; yellow: one channel; dark blue: hybrid). (a) Mean shear on the channels along the $y-$ direction halfway along the channels. (b) Pressure drop across the mechanism, measured from the inlet to the outlet. (c–e) Net force on the construct in the $x-$ (c), $y-$ (d), and $z-$ (e) directions. α-MEM, α-modified Eagle's medium [Color figure can be viewed at wileyonlinelibrary.com]

However, no significant changes were observed between forward and reverse flow directions. Lateral (x– and z–; Figure 10c,e) net forces on the construct were of negligible magnitude compared to vertical net force, suggesting that experimentally observed construct instability may be due to imperfections in the construct surface or shear separating the construct from the platen, rather than the devised flow regimes of the mechanism. A sudden change in lateral forces did occur with increasing flow rate in the reverse direction, somewhere above 5 ml/min. The geometry of the flow domain sufficiently altered the flow path to produce measurably consistent differences at the construct.

The effects of working fluid on construct stability and viability were also analyzed for the 81-channel design while varying fluid parameters, flow rate, and direction (Figure 11). As expected, measured vertical shear in the channels and net force on the construct increased with increasing fluid viscosity and aligned with the direction of flow, but otherwise behaved predictably (Figure 11a,d). Pressure drop across the mechanism behaved nearly linearly, demonstrating the possibility to estimate the amount of turbulent flow occurring in the channels as deviations from linearity between flow rate and pressure drop

(Figure 11b). Fluid viscosity also expectedly caused increases in pressure drop, while flow direction had negligible effects. Lateral forces exhibited similar, negligible behaviors to those observed while varying construct design, except that increasing fluid viscosity increased the range at which the geometry of the flow domain caused measurable changes in flow at the construct (Figure 11c,e). Lateral forces were also observed to decrease with increasing viscosity, however negligible the scale.

4 | DISCUSSION

4.1 | Fully developed flow and reduced turbulence promoted by matching platen and tissue microchannel diameters

The 81-channel pattern allows for fully developed flow since the diameters between the platen and the SSuPer tissues are the same, also discouraging significant Eddy currents. Eddy currents, indicative
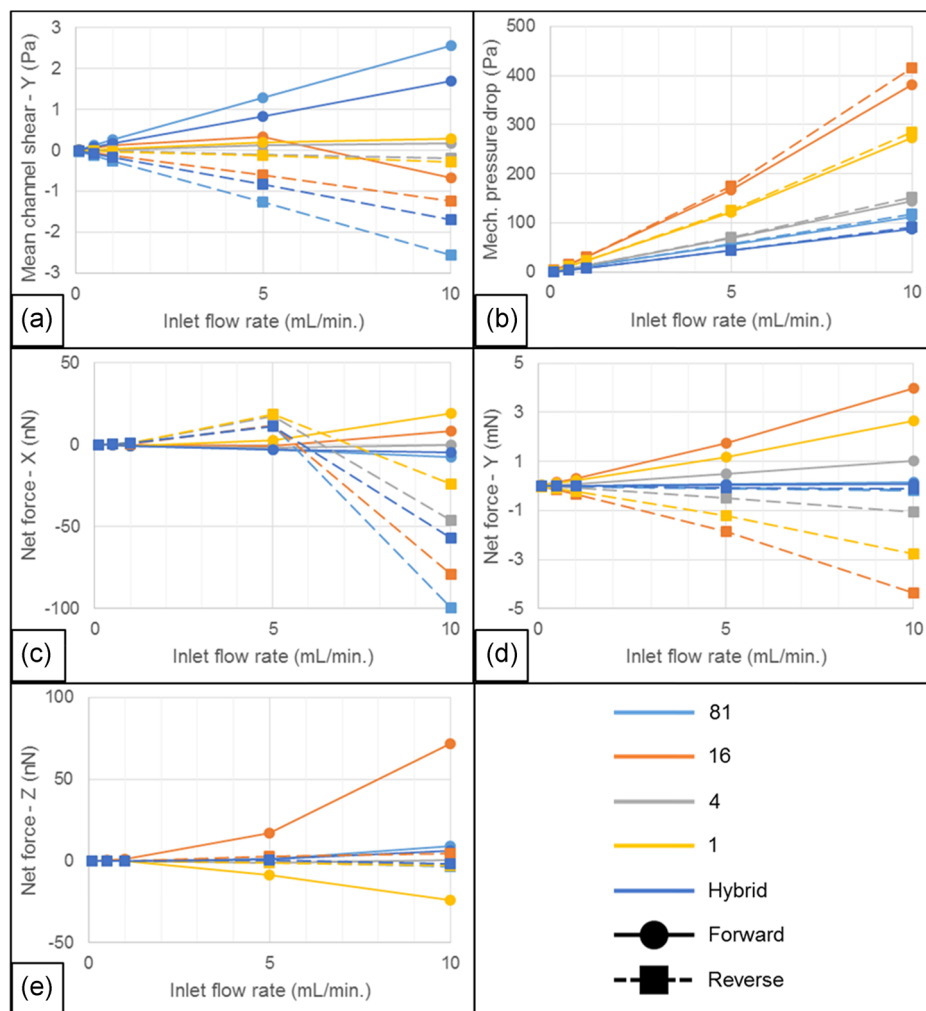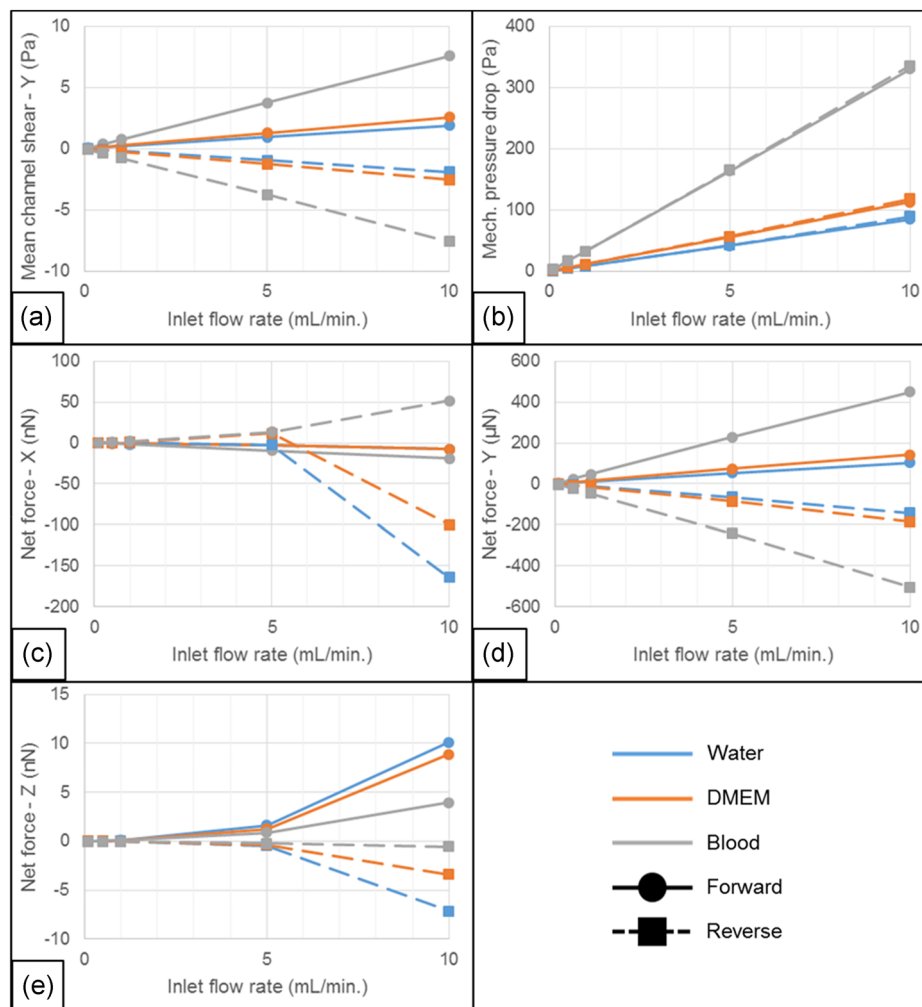

FIGURE 11 Scalar metrics of interest for 81 channels in the forward (solid, circles) and reverse (dashed, squares) directions and all working fluids (light blue: water, orange: DMEM; gray: blood). (a) Mean shear on the channels along the *y*− direction halfway along the channels. (b) Pressure drop across the mechanism, measured from the inlet to the outlet. (c–e) Net force on the construct in the *x*− (c), *y*− (d), and *z*− (e) directions [Color figure can be viewed at wileyonlinelibrary.com]

of turbulence, do not represent the predominant flow profile in vivo as turbulence is mechanically damaging to the tissue and can interfere with nutrient transfer. One approach to reducing the development of Eddy currents and achieving fully developed flow throughout the bioprinted tissue is to design SSuPer tissue pattern-matched platens to match each construct pattern. In addition, fully developed flow through the constructs can be achieved by using an appropriately thick platen, and thus microchannels. The length required to achieve this flow condition, which is normally positively correlated with channel diameter, can be determined using fluid mechanics with variables such as channel profile, viscosity, and flow rate.

4.2 | The current CFD model can account for oxygen diffusion and potential cellular oxygen consumption

The model exhibits a gradual change in oxygen concentration along the length of the tissue microchannels. Since the tissue is oxygen-saturated at steady state, the decreases in oxygen concentration are the result of oxygen consumption, indicating that the CFD model can be used to determine if tissues used in the bioreactor are receiving adequate oxygenation. The average cell oxygen consumption rate used in this model resulted in negligible reductions in oxygen concentration. However, predicted cell oxygen consumption rates span three orders of magnitude, which suggests that oxygen depletion using the current bioreactor setup may occur when using highly consumptive cell types. Increased cell densities, larger tissues, and cell proliferation within the construct (if any) after bioprint can also contribute to increased oxygen demand. Therefore, when culturing tissues in vitro, it is critical to know the oxygen consumption rate of the cells (bone cells, liver cells, etc.), resultant tissue being cultured, if proliferation is occurring, as well as the oxygen concentration in the culture medium. In some cases, as we are investigating in ongoing studies, it may be prudent to further oxygenate the medium to ensure there is oxygen available for increased cell metabolic demands.

4.3 | There are increased benefits of using "reversed" flow regarding oxygenation and tissue-platen integrity

4.3.1 | Oxygenation

As the force generated on the SSuPer tissue during forward perfusion can potentially push the tissues off of the platen, reverse flow could draw the tissue to the platen, preventing loss of the construct. The model shows that reverse flow results in minimal Eddy currents at the microchannel inlet, leading to developed flow through most of the microchannel length. However, if the tissue is not mechanically robust enough to withstand the stresses applied to it

during reverse flow, there is a possibility that the channels will collapse. A possible approach is to initiate perfusion at a very low flow rate to provide nutrient access until the construct develops sufficient integrity to support increased pressure at flow rates needed for the study.

Oxygen distributions also demonstrated that the difference in volume of the flow regions above and below the platen and construct exhibits a sort of "reservoir" effect on convection of diffusive species with respect to the larger flow region. In terms of a lumped element model, gradients of the oxygen distributions imply that the larger of the two volumes can be thought of as having a greater capacitance with respect to diffusive mass transport, the resulting distributions in which are affected by forced flow and the upper, environmental boundary. In the case of forward flow, the larger flow volume acts like a sink for diffusive mass transport of oxygen. In the case of reverse flow, the larger flow volume acts like an oxygen reservoir.

Oxygen distributions showed that the larger perfusion volume of the mechanism (above the platen) demonstrates a greater capacitance for diffusive mass transport. This finding is particularly relevant for two reasons. First, the top of the construct generally has a greater interfacial area with the larger flow volume (because the platen blocks the bottom), and increasingly so for larger constructs. While results did not demonstrate any immediate way to precisely quantify these effects, what is clear is that their effects will likely be more pronounced for larger and more metabolically demanding constructs, and for flow rates nearly too low to provide sufficient nutrient delivery. For this consideration, the upper, environmental interface provides a second control mechanism for gaseous species through control of the environment in which the entire mechanism is placed. Second, metabolic waste produced by the construct must also be removed. In the case of insufficient advection, reverse flow then likely presents the greater possibility of waste products being drawn into the construct compared to forward flow.

4.4 | Flow-induced shear stress developed in SSuPer tissue show potential for regulating cell and tissue behavior

There were, in effect, three microchannel diameters analyzed in the SSuPer tissue used as proof of concept. The fact that only tissue surrounding the smallest diameter channel exhibited mineralization supports the concept that perfusion induced shear stress can modulate osteogenesis (Sawyer et al., 2018).

Similar to cells in vivo, in vitro cell response to fluid shear is dependent on the shear level and the cell type (Wittkowske, Reilly, Lacroix, & Perrault, 2016). Osteocytes in natural bone are subject to shear stress levels between 0.8 and 3 Pa (Weinbaum, Cowin, & Zeng, 1994). MLO-Y4 cell (an early osteocyte line) exposure to fluid shear stresses in the 0.2–2 Pa range have exhibited increased osteocytic responses including ATP (Genetos, Kephart, Zhang, Yellowley, & Donahue, 2007), calcium^{2+}, (Genetos et al., 2007; Lu, Huo, Park, & Guo, 2012), Cox2 (Ponik, Triplett, & Pavalko, 2007), SOST

(X. Li et al., 2013), and osteopontin (Ponik et al., 2007) upregulation while higher fluid shear stresses (in the 3.0-Pa range) applied to MLO-Y4 cells have resulted in decreased cell viability (X. Li et al., 2013). Similarly, MLO-Y4s show decreasing RANKL and increasing COX-2 as shear increases from no flow to 1 to 5 Pa (J. Li, Rose, Frances, Sun, & You, 2012). For cardiac tissue, shear stresses greater than 0.25 Pa have been shown to cause cellular damage and reduce cell expansion (Barash et al., 2010; Brown, Iyer, & Radisic, 2008; Lecina, Ting, Choo, Reuveny, & Oh, 2010; Teo, Mantalaris, & Lim, 2012). For bone-marrow mesenchymal stem cells, a shear level of 0.5 Pa has been shown to inhibit proliferation and, in some cases, push the stem cells toward osteogenic differentiation. The average shear rates achieved for 0.1 to 10 ml/min flow in both flow directions in our 81-channel SSuPer tissue model range from 0.067 to 7.58 Pa for blood and from 0.02281 to 2.56 Pa for culture media. The shear rates achieved with our model indicate that our system should be able to provide the optimal shear environment for biofabricated bone and cardiac tissues.

Since the CFD model allows the determination of shear stress within the microchannels, a possible future study will be to test more SSuPer tissues with consistent microchannel diameters and test at increasing flow rates to determine the minimal shear rate required to invoke osteogenesis and mineralization.

5 | CONCLUSION

5.1 | Key innovations

A key innovation of the present study is the adhesive coupling of the 3D-bioprinted tissue construct to the platen while aligning the 200-μm diameter tissue microchannels with the platen microchannels. Instead of allowing the holes to close, thus limiting nutrient access to the tissue bulk, we have effectively used the needles to generate the smallest perfusible biofabricated conduits ever produced in a scaffold-free bioprinted tissue and we have also demonstrated biological activity as a result of their perfusion. Spacing between microchannels ensures nutrient access throughout the tissue (Grimes, Fletcher, & Partridge, 2014). To our knowledge, this is the first demonstration of a bioprinted tissue supporting its own weight with self-secreted matrix during continuous perfusion without support from biomaterial scaffolding. We have demonstrated, using constructs made from IDG-SW3 cell spheroids, that SSuPer tissue microchannels maintain their patency over the course of bioreactor culture (perfused or non-perfused) for up to 3 weeks (unpublished). Although Von Kossa alone is not sufficient to confirm in vitro mineralization (Bonewald et al., 2003), the localization of the staining to only the smallest channels and not the tissue perimeter suggests that phosphate staining is due to cellular deposition of mineral. Fourier transform infrared spectroscopy or other analyses should, however, be used to verify calcium phosphate presence and quality (Bonewald et al., 2003).

Although researchers have thoroughly investigated perfusion and predicted drug uptake using CFD analysis of naturally derived tissues

(d'Esposito et al., 2018), the CFD analysis of bioprinted SSuPer tissues perfused in the FABRICA bioreactor represents a new paradigm in utilizing tissue models and bioreactor platforms for research, clinical, and drug development (d'Esposito et al., 2018) applications while providing a scalable, modular, and integrated platform for tissue engineering in general. With the capability of our team to fabricate bone-like (as demonstrated in this manuscript), liver-like (Gao et al., 2001), and other tissues (in development), the great potential in the platform described is that it can be implemented with human cell-based SSuPer tissues and perfused with drugs, meaning the platform can be used for preclinical in vitro drug testing of drug candidates. Since in vivo animal models do not accurately represent human biology, the ability to test scaffold-free 3D human tissues will elucidate potential clinical outcomes while also allowing varied patient populations to be studied before testing in humans. The platform therefore has the potential to reduce drug recidivism in the clinical trial phase. Methods for producing a 3D tissue model further representative of the natural tissue include accounting for the heterocellular cell composition, and thus combination of metabolism of different cell types, as observed in natural tissues, as well as inputting CFD medium flow rates matched to the in situ flow rates for the tissue being studied.

Another exciting future approach is to include vascular cells in the tissue construct to line the microchannels to replicate the vascular cell composition and structure found in all vascularized tissues. The flow velocities implemented by the flow system and input into the CFD model are within the operational envelope of our bioreactor system and match closely with physiological vascular flow rates (Groth et al., 1995). While the range of vascular channel diameters in the natural vasculature is between 5 and 10 mm, tissue construct design was limited to the range of diameters on the original platen. Future work regarding this platform includes controllable oxygen provision, a complete study of SSuPer tissues in vitro using the FABRICA bioreactor, and data from this CFD model. In theory, however, the SSuPer tissue concept and the FABRICA are limited to neither the platen dimensions nor the Kenzan method, which means the concept can be scaled up or down to accommodate different tissue dimensions. Ongoing work therefore includes developing SSuPer tissue biofabrication methods, which do not rely on the Kenzan method, facilitating widespread adoption of SSuPer tissues as a research tool.

5.2 | SSuPer tissues approximate natural tissue structures

In bone, Haversian canal diameters vary with anatomical location and with age (Cooper et al., 2007; Cvetkovic et al., 2013). In the human femoral shaft, Haversian canal diameters can reach as high as $150.4 \pm 118.9\,\mu m$ and osteons reaching $252 \pm 24\,\mu m$ (Cooper et al., 2007; Cvetkovic et al., 2013), putting our model and construct within the anatomical range of Haversian canal diameters. However, the microchannel distribution in our construct is $6.25/mm^2$, nearly half that of the in vivo canal distribution. Per Zahm et al. (2010), a drop in oxygen

available to cells as a function of distance from the microchannel is expected but cell viablility can be maintained when a 100 mmHg oxygen partial pressure is prescribed. Our computational model matches this outcome as it appears the saturated oxygen is sufficient to support cell viability at the microchannel distribution designed into the SSuPer tissue. However, given the greater density of natural bone, it is possible that, as the density of the maturing biofabricated tissue increases closer to that of natural bone, the microchannel distribution will not be sufficient to support cell viability. In fact, Zahm et al. (2010) suggest that the size of the osteon is limited by the diffusion distance of oxygen through bone tissue surrounding the Haversian canal. The maturation of biofabricated bone may therefore call for a higher microchannel density in future constructs. To confirm this, more exhaustive studies, which are beyond the scope of the current study, should provide controlled oxygenation to investigate the oxygen availability and cell viability in the interchannel spaces at varying microchannel distributions. In addition, future studies should model the behavior of solutes of varying sizes within the tissues including metabolites such as glucose and growth factors.

Despite our study of bone in this manuscript, since the SSuPer tissue method is an adjustable system, we can modify the oxygenation concentration and tissue structure to match in vivo conditions and tissue designs, respectively. Our article on oxygenation studies wherein we control oxygen content in cell culture media and blood using our FABRICA bioreactor is currently under review.

ACKNOWLEDGMENTS

CONFLICT OF INTERESTS

The authors declare the intellectual property interests reported within this manuscript with potential financial interest. L.J.S. and B.P.M. are co-inventors of the patent pending FABRICA Bioreactor Platform and the SSuPer Tissue Platform.

AUTHOR CONTRIBUTIONS

L.J.S. led FABRICA and SSuPer tissue design, study design, and SSuPer tissue preparation, co-led analysis and manuscript preparation, and contributed to CFD model preparation. T.J.S. led CFD model preparation and design and co-led analysis, experimental design, and manuscript preparation. M.P. contributed to experimental design and SSuPer tissue preparation and analysis. B.P.M. contributed to SSuPer tissue design. P.L. contributed to experimental design. L.F.B. contributed to experimental design and SSuPer tissue preparation and analysis. B.E. contributed to experimental design and bioreactor design. A.T. contributed to CFD model preparation and co-led CFD analysis. All authors contributed to manuscript preparation.

DATA AVAILABILITY STATEMENT

SSuPer Tissue Dimensional data are provided in Supporting Information Material. FABRICA dimensional and computer-aided design data are proprietary.

ORCID

T. J. Sego http://orcid.org/0000-0002-4274-656X
Matthew Prideaux http://orcid.org/0000-0001-9211-9698
Jane Sterner http://orcid.org/0000-0002-9024-1355
Brian Paul McCarthy http://orcid.org/0000-0001-5366-7114
Ping Li http://orcid.org/0000-0003-1055-9505
Lynda F. Bonewald http://orcid.org/0000-0002-5536-9943
Burcin Ekser http://orcid.org/0000-0003-0741-8007
Andres Tovar http://orcid.org/0000-0003-2727-6587
Lester Joshua Smith http://orcid.org/0000-0003-4950-7569

REFERENCES

Aguilar, I. N., Smith, L. J., Olivos, D. J., Chu, T. M. G., Kacena, M. A., & Wagner, D. R. (2019). Scaffold-free bioprinting of mesenchymal stem cells with the regenova printer: Optimization of printing parameters. *Bioprinting, 15,* https://doi.org/10.1016/j.bprint.2019.e00048

Aguilar, I. N., Olivos, D. J., Brinker, A., Alvarez, M. B., Smith, L. J., Chu, T. M. G., … Wagner, D. R. (2019). Scaffold-free bioprinting of mesenchymal stem cells using the Regenova printer: Spheroid characterization and osteogenic differentiation. *Bioprinting, 15,* https://doi.org/10.1016/j.bprint.2019.e00050

Anton Paar. (n.d.). Viscosity of Whole Blood. Retrieved June 21, 2018, from https://wiki.anton-paar.com/en/whole-blood/

Ball, O., Nguyen, B. N. B., Placone, J. K., & Fisher, J. P. (2016). 3D printed vascular networks enhance viability in high-volume perfusion bioreactor. *Annals of Biomedical Engineering, 44*(12), 3435–3445. https://doi.org/10.1007/s10439-016-1662-y

Barash, Y., Dvir, T., Tandeitnik, P., Ruvinov, E., Guterman, H., & Cohen, S. (2010). Electric field stimulation integrated into perfusion bioreactor for cardiac tissue engineering. *Tissue Engineering Part C: Methods, 16,* 1417–1426. https://doi.org/10.1089/ten.tec.2010.0068

Blakely, A. M., Manning, K. L., Tripathi, A., & Morgan, J. R. (2015). Bio-pick, place, and perfuse: A new instrument for 3D tissue engineering. *Tissue*

Engineering. Part C, Methods, 21, 737–746. https://doi.org/10.1089/ten.TEC.2014.0439

Bonewald, L. F., Harris, S. E., Rosser, J., Dallas, M. R., Dallas, S. L., Camacho, N. P., … Boskey, A. (2003). Von Kossa staining alone is not sufficient to confirm that mineralization in vitro represents bone formation. *Calcified Tissue International*, 72, 537–547. https://doi.org/10.1007/s00223-002-1057-y

Bonfiglio, A., Leungchavaphongse, K., Repetto, R., & Siggers, J. H. (2010). Mathematical modeling of the circulation in the liver lobule. *Journal of Biomechanical Engineering*, 132(11), 111011. https://doi.org/10.1115/1.4002563

Brown, M. A., Iyer, R. K., & Radisic, M. (2008). Pulsatile perfusion bioreactor for cardiac tissue engineering. *Biotechnology Progress*, 24, 907–920. https://doi.org/10.1002/btpr.11

Carrier, R. L., Rupnick, M., Langer, R., Schoen, F. J., Freed, L. E., & Vunjak-Novakovic, G. (2002). Perfusion improves tissue architecture of engineered cardiac muscle. *Tissue Engineering*, 8, 175–188. https://doi.org/10.1089/107632702753724950

Cooper, D. M. L., Thomas, C. D. L., Clement, J. G., Turinsky, A. L., Sensen, C. W., & Hallgrímsson, B. (2007). Age-dependent change in the 3D structure of cortical porosity at the human femoral midshaft. *Bone*, 40, 957–965. https://doi.org/10.1016/j.bone.2006.11.011

Cvetkovic, V. J., Najman, S. J., Rajkovic, J. S., Zabar, A. L. J., Vasiljevic, P. J., Djordjevic, L. J. B., & Trajanovic, M. D. (2013). A comparison of the microarchitecture of lower limb long bones between some animal models and humans: A review. *Veterinarni Medicina*, 58, 339–351. https://doi.org/10.17221/6914-VETMED.

Dennis, R. G., Smith, B., Philp, A., Donnelly, K., & Baar, K. (2009). Bioreactors for guiding muscle tissue growth and development. *Adv Biochem Engin/Biotechnol*, 112, 39–79. https://doi.org/10.1007/10_2008_2

d'Esposito, A., Sweeney, P. W., Ali, M., Saleh, M., Ramasawmy, R., Roberts, T. A., … Walker-Samuel, S. (2018). Computational fluid dynamics with imaging of cleared tissue and of in vivo perfusion predicts drug uptake and treatment responses in tumours. *Nature Biomedical Engineering*, 2(10), 773–787. https://doi.org/10.1038/s41551-018-0306-y

Dimmeler, S., Haendeler, J., Rippmann, V., Nehls, M., & Zeiher, A. M. (1996). Shear stress inhibits apoptosis of human endothelial cells. *FEBS Letters*, 399, 71–74. https://doi.org/10.1016/S0014-5793(96)01289-6

Dusting, J., Sheridan, J., & Hourigan, K. (2006). A fluid dynamics approach to bioreactor design for cell and tissue culture. *Biotechnology and Bioengineering*, 94, 1196–1208. https://doi.org/10.1002/bit.20960

Egger, D., Spitz, S., Fischer, M., Handschuh, S., Glösmann, M., Friemert, B., … Kasper, C. (2017). Application of a parallelizable perfusion bioreactor for physiologic 3D cell culture. *Cells Tissues Organs*, 203, 316–326. https://doi.org/10.1159/000457792

Ferrell, R. T., & Himmelblau, D. M. (1967). Diffusion coefficients of nitrogen and oxygen in water. *Journal of Chemical and Engineering Data*, 12, 111–115. https://doi.org/10.1021/je60032a036

Fröhlich, E., Bonstingl, G., Höfler, A., Meindl, C., Leitinger, G., Pieber, T. R., & Roblegg, E. (2013). Comparison of two in vitro systems to assess cellular effects of nanoparticles-containing aerosols. *Toxicology In Vitro*, 27, 409–417. https://doi.org/10.1016/j.tiv.2012.08.008

Gan, L. M., Miocic, M., Doroudi, R., Selin-Sjöögren, L., & Jern, S. (2000). Distinct regulation of vascular endothelial growth factor in intact human conduit vessels exposed to laminar fluid shear stress and pressure. *Biochemical and Biophysical Research Communications*, 272, 490–496. https://doi.org/10.1006/bbrc.2000.2663

Gao, J., Dennis, J. E., Solchaga, L. A., Awadallah, A. S., Goldberg, V. M., & Caplan, A. I. (2001). Tissue-engineered fabrication of an osteochondral composite graft using rat bone marrow-derived mesenchymal stem cells. *Tissue Engineering*, 7(4), 363–371. https://doi.org/10.1089/10763270152436427

Gelinsky, M., Bernhardt, A., & Milan, F. (2015). Bioreactors in tissue engineering: Advances in stem cell culture and three-dimensional tissue constructs. *Engineering in Life Sciences*, 15, 670–677. https://doi.org/10.1002/elsc.201400216

Genetos, D. C., Kephart, C. J., Zhang, Y., Yellowley, C. E., & Donahue, H. J. (2007). Oscillating fluid flow activation of gap junction hemichannels induces ATP release from MLO-Y4 osteocytes. *Journal of Cellular Physiology*, 212, 207–214. https://doi.org/10.1002/jcp.21021

Goldstein, A. S., Juarez, T. M., Helmke, C. D., Gustin, M. C., & Mikos, A. G. (2001). Effect of convection on osteoblastic cell growth and function in biodegradable polymer foam scaffolds. *Biomaterials*, 22, 1279–1288. https://doi.org/10.1016/S0142-9612(00)00280-5

Goldstick, T. K., Ciuryla, V. T., & Zuckerman, L. (1976). Diffusion of oxygen in plasma and blood. *Advances in Experimental Medicine and Biology*, 75, 183–190.

Grimes, D. R., Fletcher, A. G., & Partridge, M. (2014). Oxygen consumption dynamics in steady-state tumour models. *Royal Society Open Science*, 1, 140080. https://doi.org/10.1098/rsos.140080

Groth, D. S., Zink, F. E., Felmlee, J. P., Kofler, J. M., James, E. M., Lindsey, J. R., & Pavlicek, W. (1995). Blood flow velocity measurements: A comparison of 25 clinical ultrasonographic units. *Journal of Ultrasound in Medicine: Official Journal of the American Institute of Ultrasound in Medicine*, 14, 273–277. https://doi.org/10.7863/jum.1995.14.4.273

Guller, A. E., Grebenyuk, P. N., Shekhter, A. B., Zvyagin, A. V., & Deyev, S. M. (2016). Bioreactor-based tumor tissue engineering. *Acta Naturae*, 8, 44–58.

Itoh, M., Nakayama, K., Noguchi, R., Kamohara, K., Furukawa, K., Uchihashi, K., … Morita, S. (2015). Scaffold-free tubular tissues created by a bio-3D printer undergo remodeling and endothelialization when implanted in rat aortae. *PLoS One*, https://doi.org/10.1371/journal.pone.0136681

Kang, Y., & Chang, J. (2018). Channels in a porous scaffold: A new player for vascularization. *Regenerative Medicine*, 13, 705–715. https://doi.org/10.2217/rme-2018-0022

Kato, Y., Boskey, A., Spevak, L., Dallas, M., Hori, M., & Bonewald, L. F. (2001). Establishment of an osteoid preosteocyte-like cell MLO-A5 that spontaneously mineralizes in culture. *Journal of Bone and Mineral Research*, 16, 1622–1633. https://doi.org/10.1359/jbmr.2001.16.9.1622

Kim, Y. J., Sah, R. L. Y., Grodzinsky, A. J., Plaas, A. H. K., & Sandy, J. D. (1994). Mechanical regulation of cartilage biosynthetic behavior: Physical stimuli. *Archives of Biochemistry and Biophysics*, 311, 1–12. https://doi.org/10.1006/abbi.1994.1201

Lecina, M., Ting, S., Choo, A., Reuveny, S., & Oh, S. (2010). Scalable platform for human embryonic stem cell differentiation to cardiomyocytes in suspended microcarrier cultures. *Tissue Engineering – Part C: Methods*, 16, 1609–1619. https://doi.org/10.1089/ten.tec.2010.0104

Li, J., Rose, E., Frances, D., Sun, Y., & You, L. (2012). Effect of oscillating fluid flow stimulation on osteocyte mRNA expression. *Journal of Biomechanics*, 45, 247–251. https://doi.org/10.1016/j.jbiomech.2011.10.037

Li, X., Liu, C., Li, P., Li, S., Zhao, Z., Chen, Y., … Zhang, D. (2013). Connexin 43 is a potential regulator in fluid shear stress-induced signal transduction in osteocytes. *Journal of Orthopaedic Research*, 31, 1959–1965. https://doi.org/10.1002/jor.22448

Lu, X. L., Huo, B., Park, M., & Guo, X. E. (2012). Calcium response in osteocytic networks under steady and oscillatory fluid flow. *Bone*, 51, 466–473. https://doi.org/10.1016/j.bone.2012.05.021

Maidhof, R., Tandon, N., Lee, E. J., Luo, J., Duan, Y., Yeager, K., … Vunjak-Novakovic, G. (2012). Biomimetic perfusion and electrical stimulation applied in concert improved the assembly of engineered cardiac tissue. *Journal of Tissue Engineering and Regenerative Medicine*, 6, e12–e23. https://doi.org/10.1002/term.525

McMurtrey, R. J. (2016). Analytic models of oxygen and nutrient diffusion, metabolism dynamics, and architecture optimization in three-dimensional tissue constructs with applications and insights in cerebral organoids. *Tissue Engineering Part C: Methods*, 22, 221–249. https://doi.org/10.1089/ten.tec.2015.0375

Moldovan, N. I. (2018). Progress in scaffold-free bioprinting for cardiovascular medicine. *Journal of Cellular and Molecular Medicine*, 22, 2964–2969. https://doi.org/10.1111/jcmm.13598

Moldovan, N. I., Hibino, N., & Nakayama, K. (2017). Principles of the Kenzan method for robotic cell spheroid-based three-dimensional bioprinting. *Tissue Engineering Part B: Reviews*, 23, 237–244. https://doi.org/10.1089/ten.teb.2016.0322

Murata, D., Tokunaga, S., Tamura, T., Kawaguchi, H., Miyoshi, N., Fujiki, M., … Misumi, K. (2015). A preliminary study of osteochondral regeneration using a scaffold-free three-dimensional construct of porcine adipose tissue-derived mesenchymal stem cells. *Journal of Orthopaedic Surgery and Research*, 10, 35. https://doi.org/10.1186/s13018-015-0173-0

Ozbolat, I. T. (2015). Scaffold-based or scaffold-free bioprinting: Competing or complementing approaches? *Journal of Nanotechnology in Engineering and Medicine*, 6(2), 024701. https://doi.org/10.1115/1.4030414

Ponik, S. M., Triplett, J. W., & Pavalko, F. M. (2007). Osteoblasts and osteocytes respond differently to oscillatory and unidirectional fluid flow profiles. *Journal of Cellular Biochemistry*, 100, 794–807. https://doi.org/10.1002/jcb.21089

Porter, B. D., Lin, A. S. P., Peister, A., Hutmacher, D., & Guldberg, R. E. (2007). Noninvasive image analysis of 3D construct mineralization in a perfusion bioreactor. *Biomaterials*, 28, 2525–2533. https://doi.org/10.1016/j.biomaterials.2007.01.013

Radisic, M., Park, H., Shing, H., Consi, T., Schoen, F. J., Langer, R., … Vunjak-Novakovic, G. (2004). Functional assembly of engineered myocardium by electrical stimulation of cardiac myocytes cultured on scaffolds. *Proceedings of the National Academy of Sciences of the United States of America*, 101, 18129–18134. https://doi.org/10.1073/pnas.0407817101

Sawyer, S. W., Shridhar, S. V., Zhang, K., Albrecht, L. D., Filip, A. B., Horton, J. A., & Soman, P. (2018). Perfusion directed 3D mineral formation within cell-laden hydrogels. *Biofabrication*, 10, 035013. https://doi.org/10.1088/1758-5090/aacb42

Sikavitsas, V. I., Bancroft, G. N., & Mikos, A. G. (2002). Formation of three-dimensional cell/polymer constructs for bone tissue engineering in a spinner flask and a rotating wall vessel bioreactor. *Journal of Biomedical Materials Research*, 62, 136–148. https://doi.org/10.1002/jbm.10150

Smith, L. J., Li, P., Holland, M. R., & Ekser, B. (2018). FABRICA: A bioreactor platform for printing, perfusing, observing, & stimulating 3D tissues. *Scientific Reports*, 8(1), 7561. https://doi.org/10.1038/s41598-018-25663-7

Sniegoski, L. T., & Moody, J. R. (1979). Determination of serum and blood densities. *Analytical Chemistry*, 51, 1577–1578. https://doi.org/10.1021/ac50045a052

Stiehler, M., Bunger, C., Baatrup, A., Lind, M., Kassem, M., Mygind, T., … Mygind, T. (2009). Effect of dynamic 3-D culture on proliferation, distribution, and osteogenic differentiation of human mesenchymal stem cells. *Journal of Biomedical Materials Research – Part A*, 89, 96–107. https://doi.org/10.1002/jbm.a.31967

Teo, A., Mantalaris, A., & Lim, M. (2012). Hydrodynamics and bioprocess considerations in designing bioreactors for cardiac tissue engineering. *Journal of Regenerative Medicine and Tissue Engineering*, 1, 4. https://doi.org/10.7243/2050-1218-1-4

Toratani, T., Nakase, J., Numata, H., Oshima, T., Takata, Y., Nakayama, K., & Tsuchiya, H. (2017). Scaffold-free tissue-engineered allogenic adipose-derived stem cells promote meniscus healing. *Arthroscopy – Journal of Arthroscopic and Related Surgery*, 33, 346–354. https://doi.org/10.1016/j.arthro.2016.07.015

Viscosity of Water. (2018). Retrieved June 21, 2018, from https://wiki.anton-paar.com/en/water/

Wang, T. W., Wu, H. C., Wang, H. Y., Lin, F. H., & Sun, J. S. (2009). Regulation of adult human mesenchymal stem cells into osteogenic and chondrogenic lineages by different bioreactor systems. *Journal of Biomedical Materials Research – Part A*, 88, 935–946. https://doi.org/10.1002/jbm.a.31914

Warren, S. M., Sailon, A. M., Allori, A. C., Davidson, E. H., Reformat, D. D., & Allen, R. J. (2009). A novel flow-perfusion bioreactor supports 3D dynamic cell culture. *Journal of Biomedicine and Biotechnology*, 873816. https://doi.org/10.1155/2009/873816

Weinbaum, S., Cowin, S. C., & Zeng, Y. (1994). A model for the excitation of osteocytes by mechanical loading-induced bone fluid shear stresses. *Journal of Biomechanics*, 27, 339–360. https://doi.org/10.1016/0021-9290(94)90010-8

Wittkowske, C., Reilly, G. C., Lacroix, D., & Perrault, C. M. (2016). In vitro bone cell models: Impact of fluid shear stress on bone formation. *Frontiers in Bioengineering and Biotechnology*, 4, https://doi.org/10.3389/fbioe.2016.00087

Wu, P. K., & Ringeisen, B. R. (2010). Development of human umbilical vein endothelial cell (HUVEC) and human umbilical vein smooth muscle cell (HUVSMC) branch/stem structures on hydrogel layers via biological laser printing (BioLP). *Biofabrication*, 2, 014111. https://doi.org/10.1088/1758-5082/2/1/014111

Ye, H., Xia, Z., Ferguson, D. J. P., Triffitt, J. T., & Cui, Z. (2007). Studies on the use of hollow fibre membrane bioreactors for tissue generation by using rat bone marrow fibroblastic cells and a composite scaffold. *Journal of Materials Science: Materials in Medicine*, 18(4), 641–648. https://doi.org/10.1007/s10856-007-2314-4

Zahm, A. M., Bucaro, M. a, Ayyaswamy, P. S., Srinivas, V., Shapiro, I. M., Adams, C. S., & Mukundakrishnan, K. (2010). Numerical modeling of oxygen distributions in cortical and cancellous bone: Oxygen availability governs osteonal and trabecular dimensions. *American Journal of Physiology Cell Physiology*, 299, C922–C929. https://doi.org/10.1152/ajpcell.00465.2009

Zhang, Y., Wu, X., Wang, Y., Zhu, S., Gao, B. Z., & Yuan, X. C. (2014). Measurement of the microscopic viscosities of microfluids with a dynamic optical tweezers system. *Laser Physics*, 24, 065601. https://doi.org/10.1088/1054-660X/24/6/065601

Zhou, Y., Shen, J. X., & Lauschke, V. M. (2019). Comprehensive evaluation of organotypic and microphysiological liver models for prediction of drug-induced liver injury. *Frontiers in Pharmacology*, 10, https://doi.org/10.3389/fphar.2019.01093

SUPPORTING INFORMATION

Additional supporting information may be found online in the Supporting Information section.